# FURTHER-FC

**F**urther **U**nderstanding **R**elated to **T**ransport limitations at **H**igh current density towards future **E**lect**R**odes for **F**uel **C**ells

## Multiscale Modelling

T. Jahnke (DLR), K. Gülicher (DLR), K. Karan (UCA), M. Maloum (INPT), M. Prat (INPT), M. Quintard (INPT), P. Schott (CEA) , J. Pauchet (CEA)

# Content of the presentation

1. Objectives multiscale modeling
2. Modeling of ionomer films with MD
3. Modeling of catalyst layer on sub-µm scale
4. Microstructure resolved modeling of GDL/MPL and CCL
5. Single cell modeling

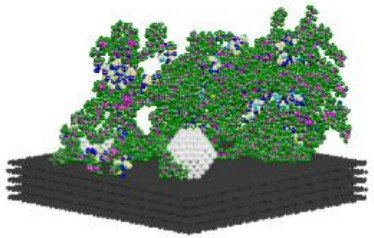

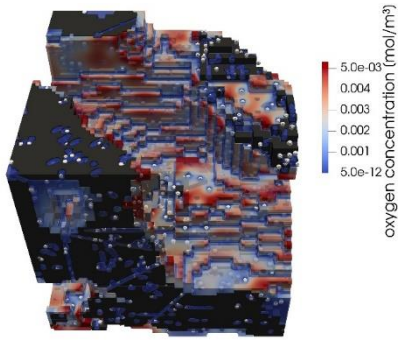


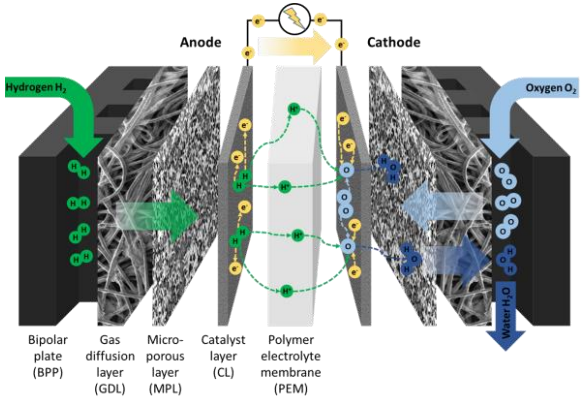


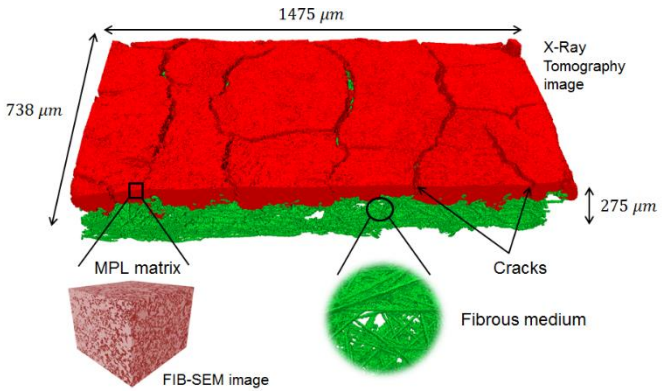


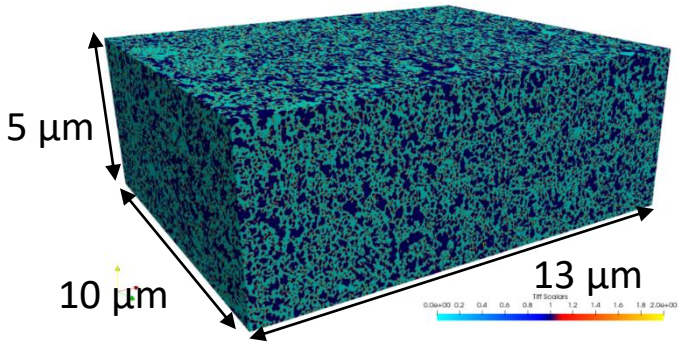

# Objectives of the work described

**Main objectives:**

- Improved understanding of performance limitations by modeling of processes in the cathode catalyst layer at all relevant scales:
  - In the ionomer film with Molecular Dynamics
  - On the sub-micrometer scale with Lattice-Boltzmann modeling
  - On the single layer scale with Direct Numerical Simulation (DNS)
  - On the cell scale with volume averaged models
- Development of multiscale modeling approach to connect lower scale mechanisms/material properties with cell performance
- Simulation-based interpretation of experimental observations

# MD simulations of the ionomer film

- **Objectives:**
  - Simulation of representative ionomer film structures in catalyst layer using Molecular Dynamics (MD)
  - Determination of the oxygen and water transport in/transfer to the ionomer films
  - Investigation of performance limiting processes on ionomer scale (poisoning by sulphonic group; Pt/ionomer interfacial water)
  - Simulation of water contact angle on ionomer surface

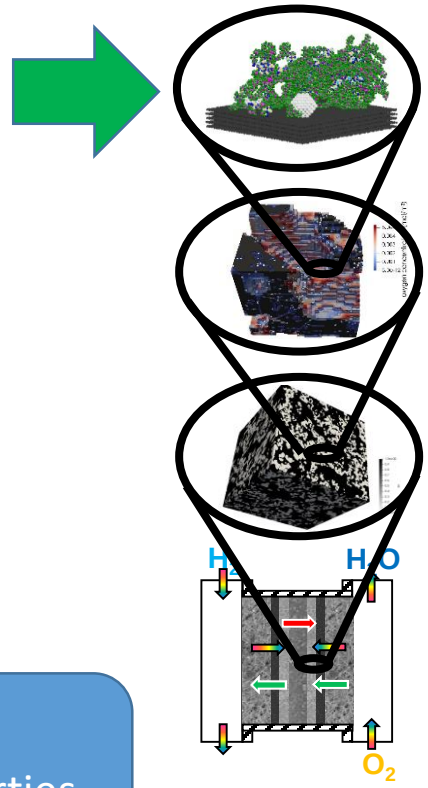


**Input**
AFM analysis of ionomer properties

→

Molecular Dynamics simulation

→

**Output**
Transport properties of ionomer film

# MD simulations of the ionomer film

- **Results:**
  - Ionomer self-assembly process for different substrates and different dispersions (water, isopropyl alcohol (IPA) and water-IPA mixture) simulated
  - Abundance of sulphonic groups at ionomer/Pt interface even in ink/dispersion media

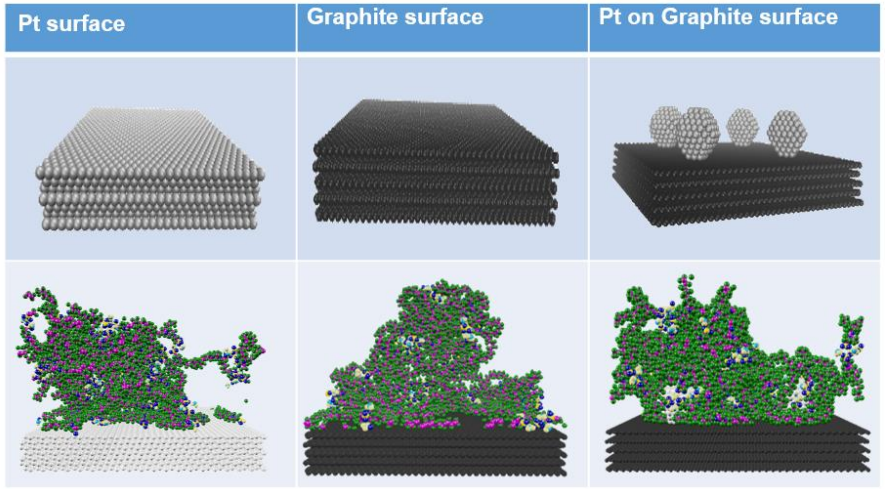


Self-assembly on different substrates in IPA

  - Simulation of solvent evaporation confirm ionic cluster formation

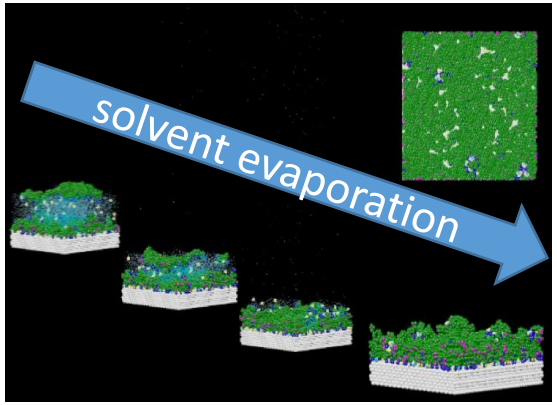


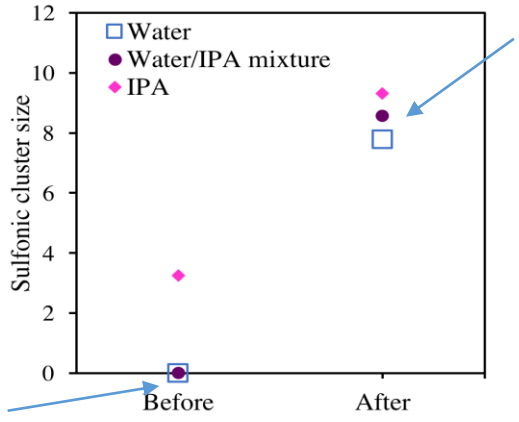


Drier film has 8-10 ion pairs (SO3-/H+) in a cluster or domain

No ionic cluster in self-assembled films (think ink stage) in water and water/IPA dispersions

# MD simulations of the ionomer film

- **Results:**
  - Limited work could be done on oxygen transport properties of the ionomer film due to lack of funding at UCA
  - Preliminary calculations of oxygen density show similar trends as published by Jinnouchi et al. (2016): Oxygen density peaks at the Nafion/vapor free interface
  - Water enrichment at Pt/Nafion interface which has multiple implications – facile proton transport (?), additional O2 transport due to water layer (?), and low local pH.

    → to be investigated in future work

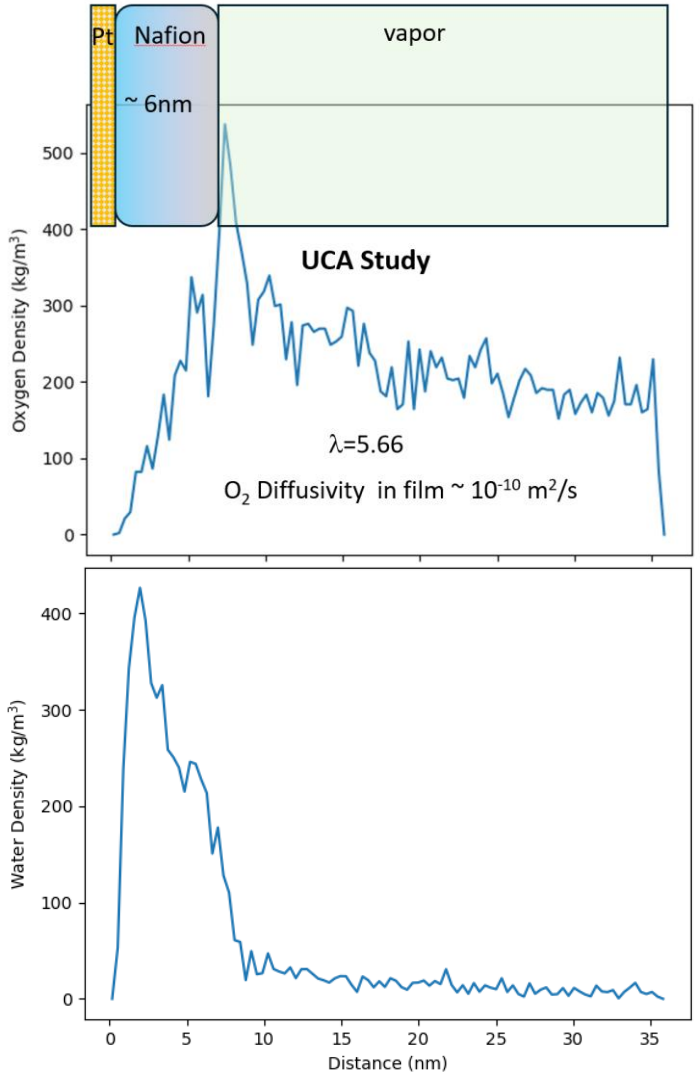

# CCL on sub-micrometer scale

- **Objectives:**
  - Identification of local transport losses on sub-µm scale
  - Development of Lattice Boltzmann model for coupled transport and electrochemistry
  - Derivation of effective local transport resistance distributions
  - Investigations on the effect of CCL microstructure

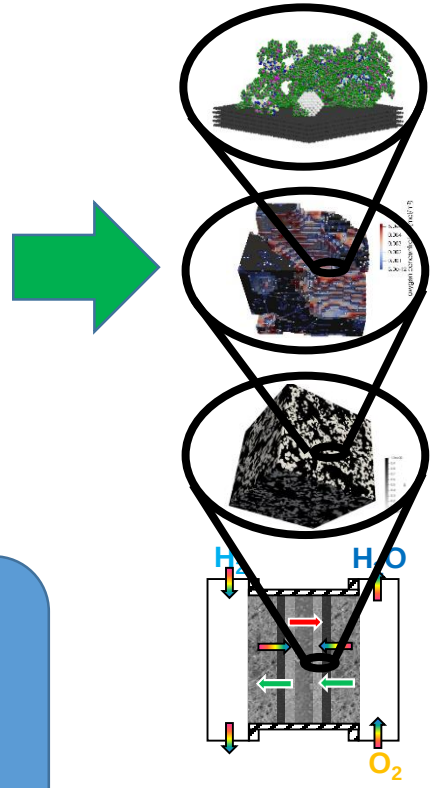


**Inputs**
- Catalyst microstructure
- Catalyst and ionomer distribution
- Contact angles
- Properties of the ionomer depending on the water content
- Local conditions in CCL

→ Lattice Boltzmann →

**Output**
Microstructure-dependent local transport resistance

# CCL on sub-micrometer scale

- **Lattice Boltzmann model**
  - MRT LBM[1] for **diffusion of oxygen in primary and secondary pores and ionomer**:

$$f_\alpha(x + c_\alpha \Delta t, t + \Delta t) = f_\alpha(x,t) + Q^{-1}\Lambda Q\left(f_{\alpha(x,t)} - f_\alpha^{\mathrm{eq}}(x,t)\right)$$

  - **Sorption processes** with finite kinetics at interfaces (gas|ionomer, gas|water, ionomer|platinum)

$$f_\alpha(x_\mathrm{A}, t+\Delta t) = \frac{1}{-\frac{1}{4}\frac{1}{k_\mathrm{dis}}\frac{\Delta x}{\Delta t} - \frac{1}{H} - 1}\left[\left(-\frac{1}{4}\frac{1}{k_\mathrm{dis}}\frac{\Delta x}{\Delta t} + \frac{1}{H} - 1\right)\hat{f}_{\bar\alpha}(x_\mathrm{A},t) - 2\hat{f}_\alpha(x_\mathrm{B},t)\right],$$

$$f_{\bar\alpha}(x_\mathrm{B}, t+\Delta t) = \frac{1}{-\frac{1}{4}\frac{1}{k_\mathrm{dis}}\frac{\Delta x}{\Delta t} - \frac{1}{H} - 1}\left[\left(-\frac{1}{4}\frac{1}{k_\mathrm{dis}}\frac{\Delta x}{\Delta t} - \frac{1}{H} + 1\right)\hat{f}_\alpha(x_\mathrm{B},t) - \frac{2}{H}\hat{f}_{\bar\alpha}(x_\mathrm{A},t)\right]$$

  - **ORR at platinum surfaces** realized as modified bounce back condition[2]

$$f_\alpha^{\mathrm{O}_2} = (1 - k_\mathrm{LB}) f_{\bar\alpha}^{\mathrm{O}_2},$$

$$k_\mathrm{LB} = \left(\frac{8 k_\mathrm{ORR}\Delta t}{\Delta x}\right) \Big/ \left(1 + \frac{k_\mathrm{ORR}\Delta x}{2 D_\mathrm{N}}\right)$$

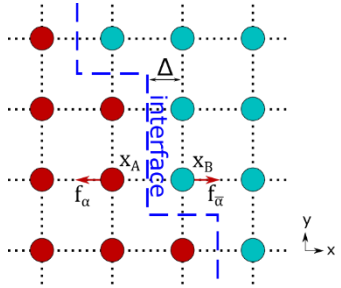


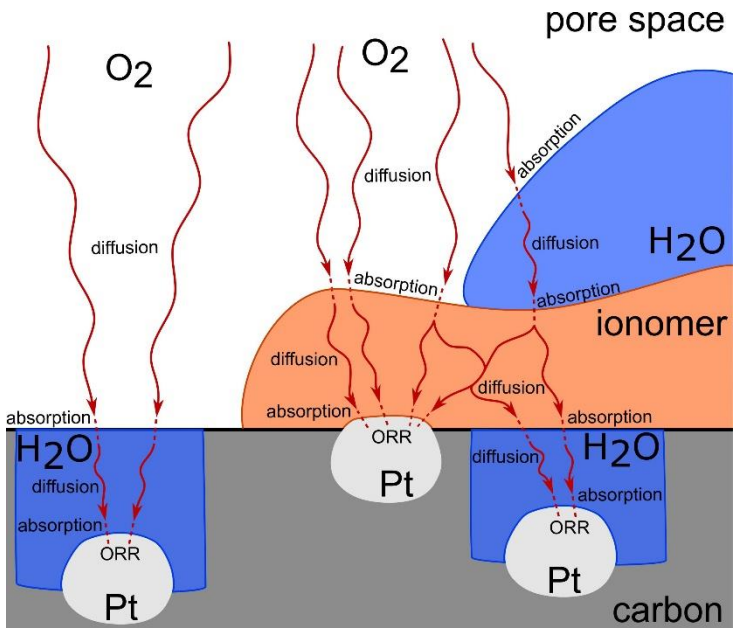


- **Output**: local transport resistance distribution $N(R_\mathrm{Pt})$ depending on CCL microstructure, where $R_\mathrm{Pt} = \frac{4Fc_g}{H\, i_\mathrm{lim}}$


[1] Chen, L., Zhang, R., Kang, Q., Tao, W. Q. (2020), Chemical Engineering Journal, **391**, 123590
[2] Molaeimanesh, G. R., Akbari, M. H. (2015), International Journal of Hydrogen Energy, **40**, 5169

# CCL on sub-micrometer scale

- **Ionomer properties**
  - from **literature** and **experiments**
  - **diffusion coefficient** for oxygen in ionomer[1]
  - **Henry's constant** for oxygen absorption by ionomer[1]
  - **Ionomer oxygen transport resistance** from CEA
  - experiment: only **total** interface resistance

$$R_{\mathrm{Io}} = H_{\mathrm{Io}}/k_{\mathrm{Io}} = H_{\mathrm{Io}}\left(1/k_{\mathrm{P,Io}} + 1/k_{\mathrm{Io,Pt}}\right)$$

  - in simulations: **contribution** of interfaces

$$k_{\mathrm{P,Io}} = H_{\mathrm{P,Io}}/(\kappa R_{\mathrm{Io}}),$$

$$k_{\mathrm{Io,Pt}} = H_{\mathrm{P,Io}}/\left((1-\kappa)R_{\mathrm{Io}}\right)$$

  - (in planar geometry, total resistance remains equal)

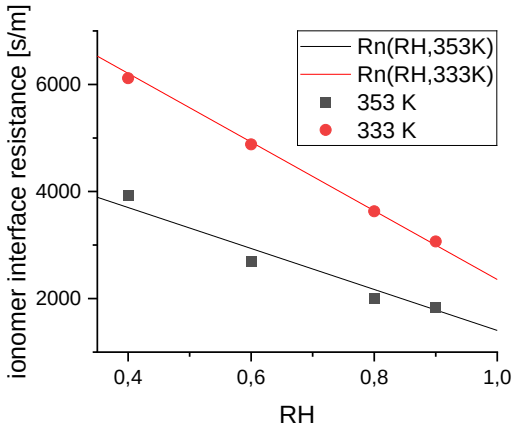


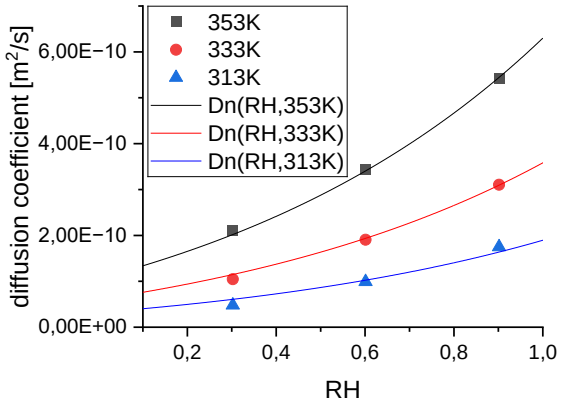


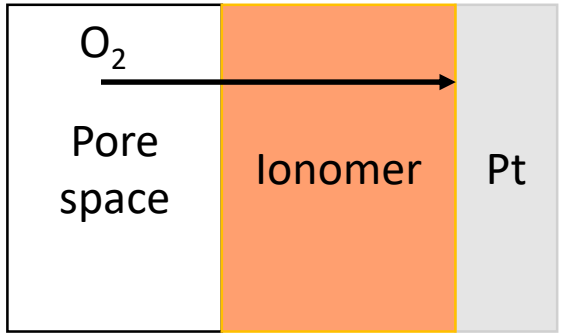


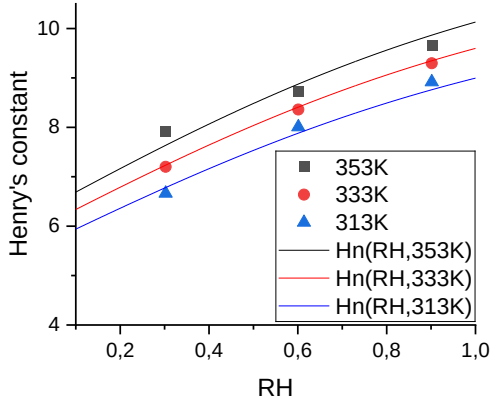


[1]: K. Kudo, R. Jinnouchi, Y. Morimoto, Electrochimica Acta 209, (2016) 682

# CCL on sub-micrometer scale

- Distribution of **micro pores:**
  - start from **reconstruction** of carbon and ionomer based on FIB-SEM[1]
  - Calculation of **micro porosity**

$$\varepsilon_{micro} = \frac{V_{micro}}{V_{micro}+V_c} = 1 - \frac{\left(\frac{1}{\eta_{Pt}}-1\right)\frac{A_{CCL}\mu_{Pt}}{\varrho_c}}{(1-\varepsilon_{macro})V_{CCL} - A_{CCL}\frac{\mu_{Pt}}{\varrho_{Pt}} - \frac{I\,\varrho_c}{C\varrho_{Io}}\left(\frac{1}{\eta_{Pt}}-1\right)\frac{A_{CCL}\mu_{Pt}}{\varrho_c}}$$

  - **Average pore size** 3.125 nm diameter
  - **Internal carbon surface area** 446 $m^2/g$
  - Distribution of **pores at carbon surface**
    - distributed randomly just below the surface of carbon
    - have small external entrance
  - Distribution of **pores inside carbon**
    - with overlap to preexistent micro pores
    - completely inside the original carbon
    - replace original carbon with micro pores **until** desired **micro porosity** is achieved

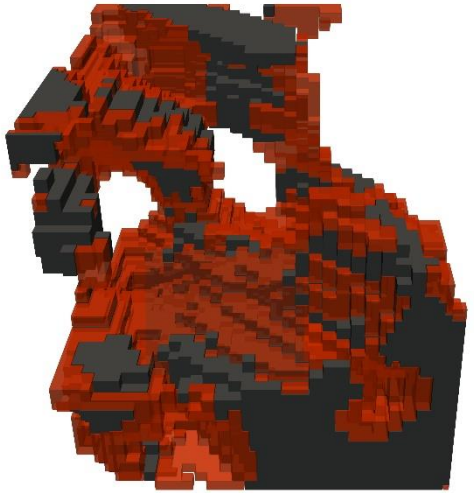

ionomer distribution

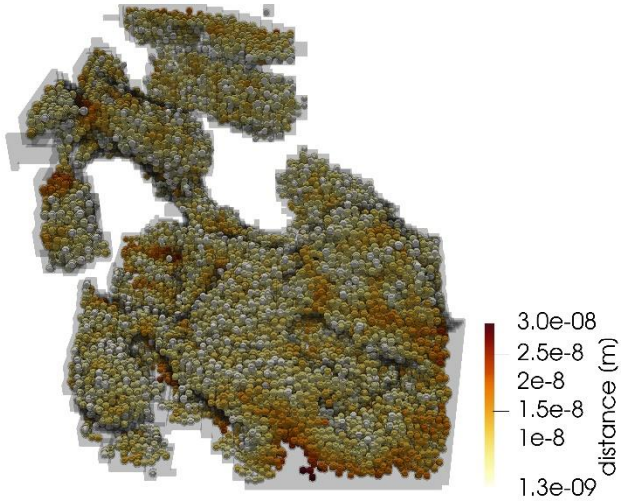


micro pores

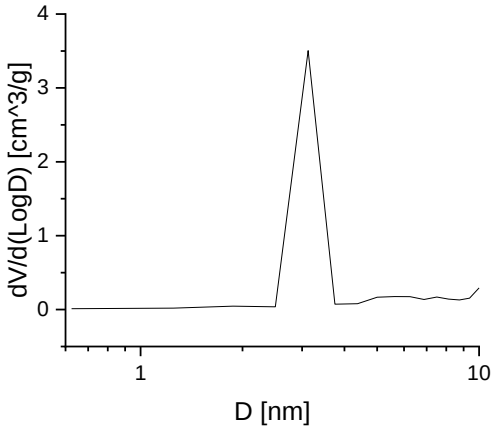


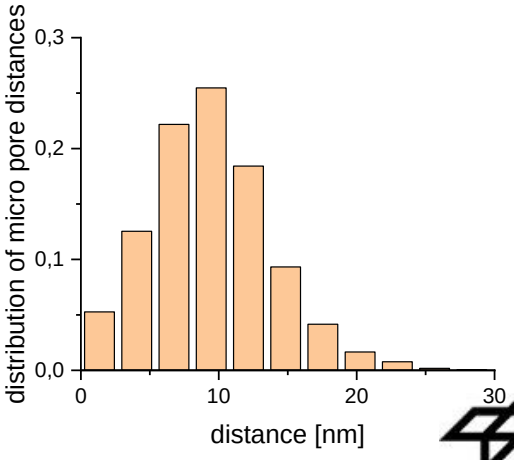


[1]: M. Ahmed-Maloum et al., International Journal of Hydrogen Energy 80 (2024) 39–56

# CCL on sub-micrometer scale

- Distribution of **platinum particles:**
  - distinction between internal|external platinum
  - **internal Pt:**
    - radius 1.2nm
    - 82% of **Pt particles**
    - 70% of **total Pt surface**
    - 74% of ECSA
  - **external Pt:**
    - radius 1.6nm
    - 18% of **Pt particles**
    - 30% of **total Pt surface**
    - 26% of ECSA (because only 80% ionomer coverage)
  - increase number of distributed platinum particles until **Pt loading** 0.2mg/cm$^2$ is achieved
  - thereby, distribute 81% **internally**, 19% **externally**
  - platinum particles randomly distributed on external|internal carbon surface
  - Finally, move external|internal particles in/out of carbon structure until **roughness factor** of 140m$^2$/m$^2$

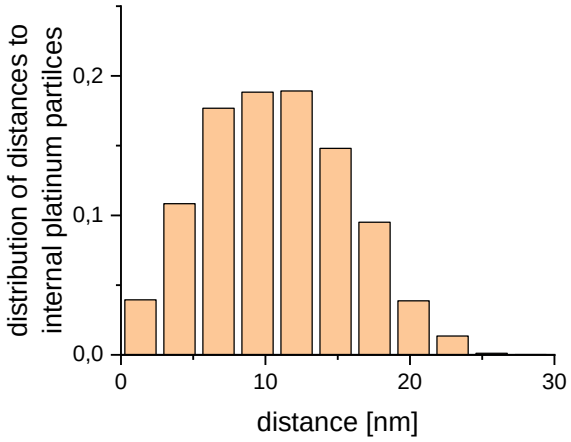


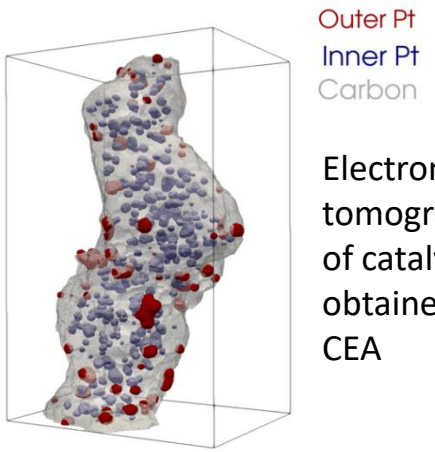


Electron tomography of catalyst obtained by CEA

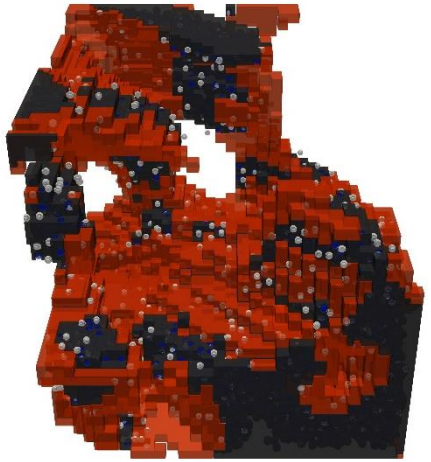

final geometry

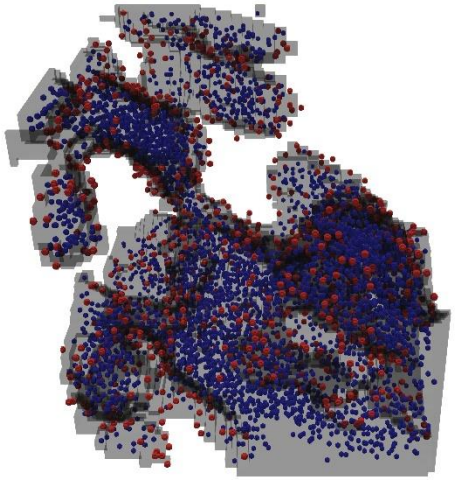

platinum particles

# CCL on sub-micrometer scale

- Liquid water distribution due to capillary condensation
  - in **macro pores**
  - **pore size distribution** estimated using GeoDict
  - **size threshold** for flooded pores from RH of air:

$$r_{\mathrm{cap}}(RH) = -2v_m \frac{s(T)}{RT\log(RH)} \cos(\theta)$$

  - with surface tension $s(T)$ from [2]

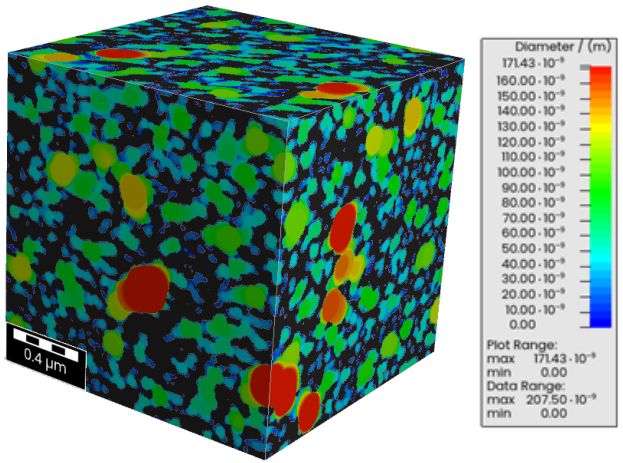


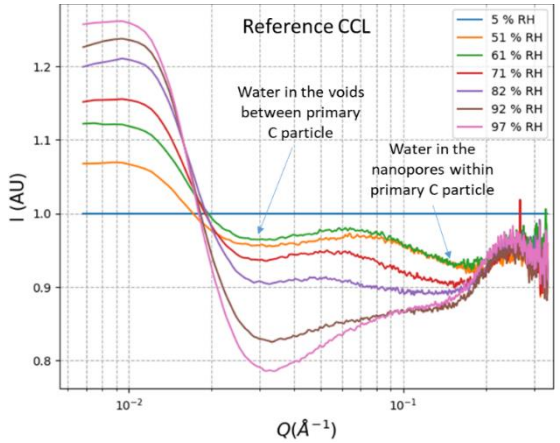


SAXS measurements (CEA) show capillary condensation in primary and secondary pores

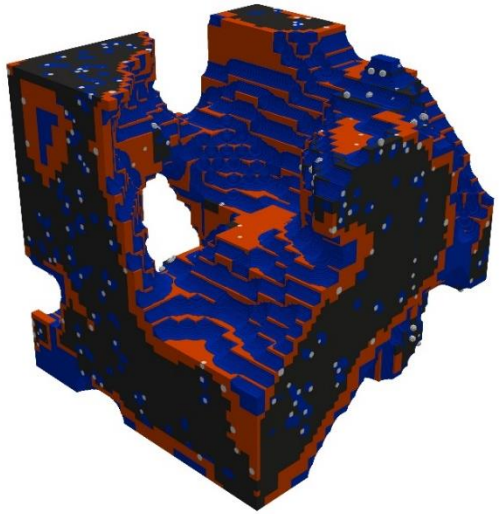

Example: $\theta = 65°$; RH = 95%

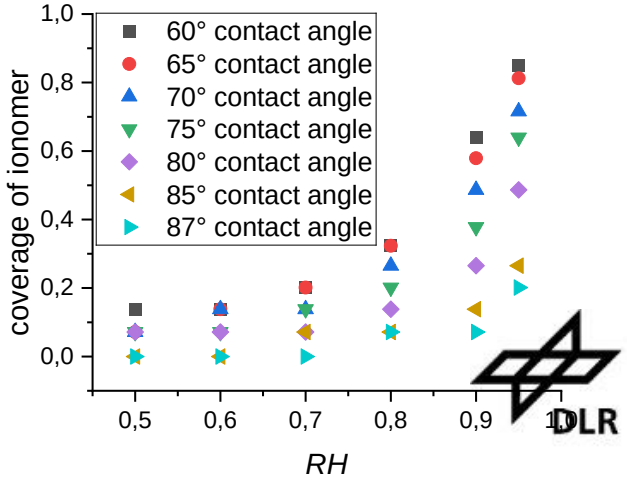


[2] Teitelbaum, B.Y., Gertolova, T.A., Siederova, E.E. (1951), Zh. Fiz. Khim., **25**, 911

# CCL on sub-micrometer scale

- **Results LBM**
  - Definition of **transport resistance** in different media:

$$R_{\mathrm{Pt}}^{\mathrm{med}} = \frac{4F\,c_{\mathrm{g}}}{H^{\mathrm{med}}\; i_{\mathrm{lim}}^{\mathrm{Pt,med}}}$$

  - Calculated from
    - arising limiting current per platinum area $i_{\mathrm{lim}}^{\mathrm{Pt,med}}$
    - entering oxygen concentration in pore space $c_{\mathrm{g}}$
  - Simulation of reference MEA:

→ average resistance for internal/external Pt

→ influence of RH

→ effect of distribution of interfacial resistance

→ broad distribution of local transport resistances

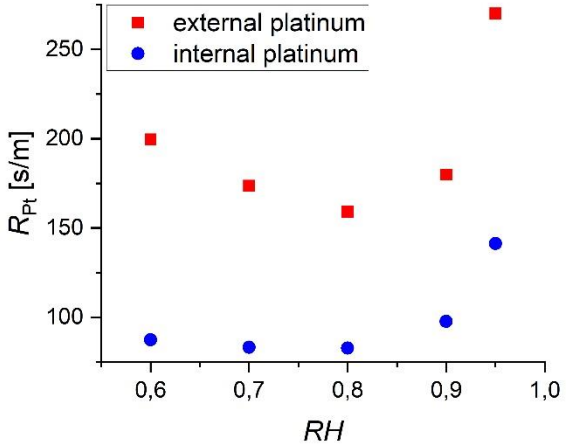


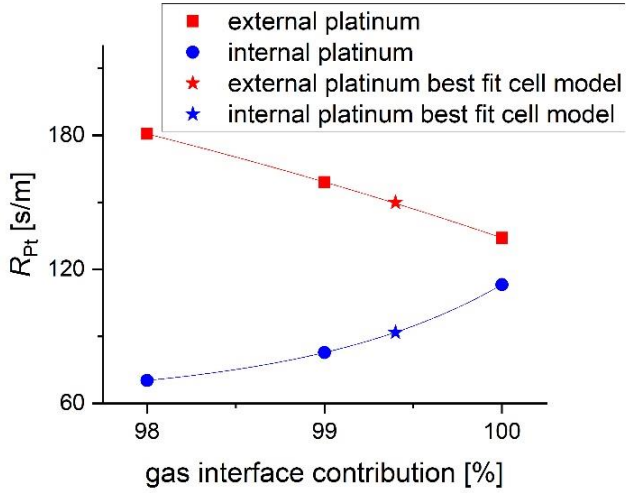


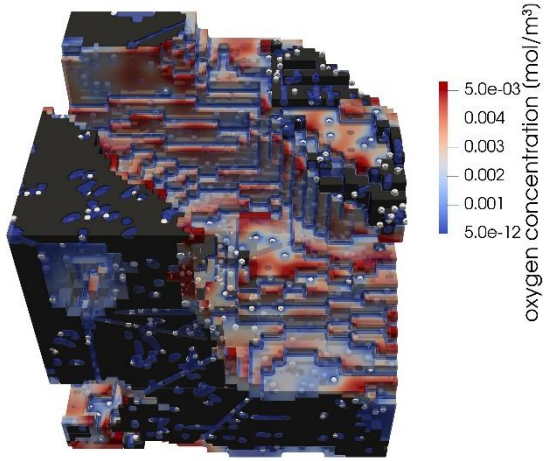


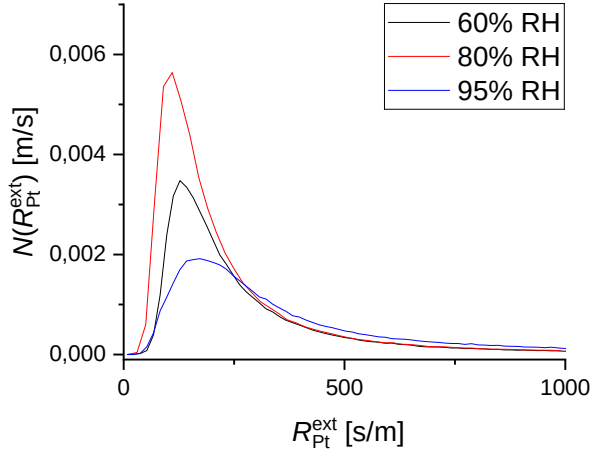


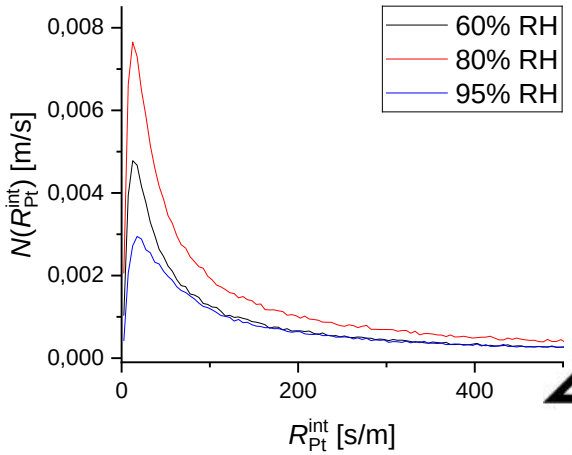


Resistance distributions as function of RH

# CCL on sub-micrometer scale

- **Results LBM**
  - Application to different CCL materials:
  - Graphitized carbon vs. HSAC → No micropores in graph. carbon; Pt distributed on carbon surface
  - HOPI vs. D2020 → Assume same microstructures but different ionomer properties (Henry constant, interfacial resistance)

$$H^{\mathrm{HOPI}} = \frac{H^{\mathrm{D2020}}}{2}, \quad R_{\mathrm{int}}^{\mathrm{HOPI}} = \frac{R_{\mathrm{int}}^{\mathrm{D2020}}}{2}$$

→ large variations in literature values[1,2]/experiments

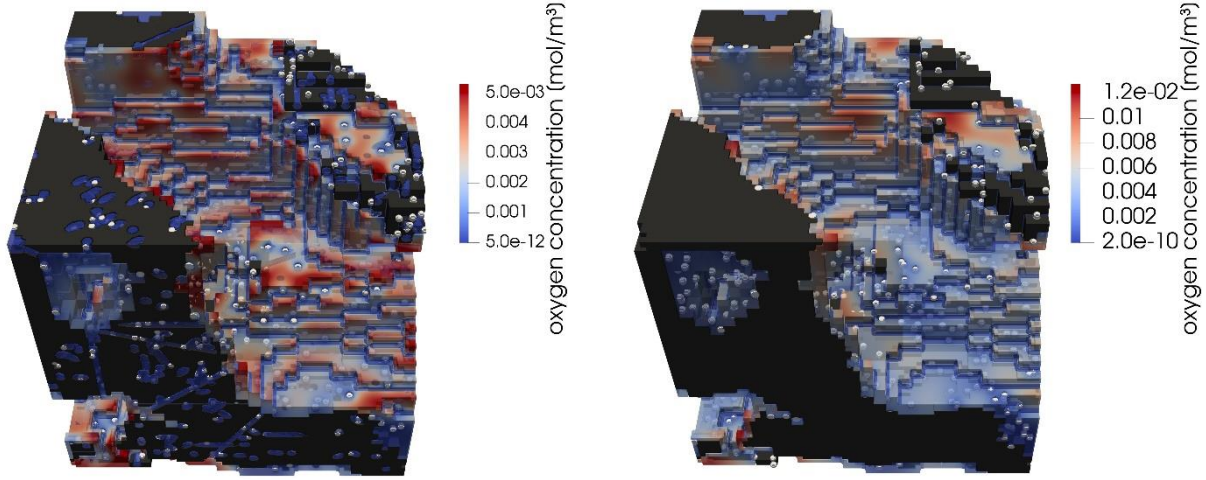


HSAC graph. carbon

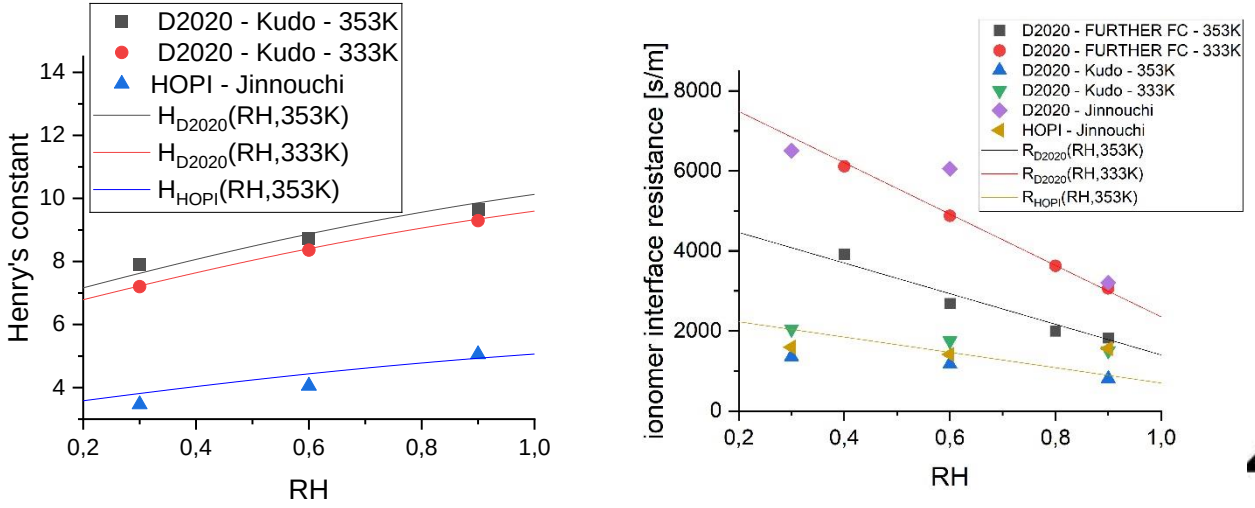


Plot ionomer properties D2020 vs HOPI


[1]: K. Kudo, R. Jinnouchi, Y. Morimoto, Electrochimica Acta 209, (2016) 682
[2]: R. Jinnouchi et al., Nature Communications 12 (2021) 4956

# Single layer scale

- **Objectives:**
  - Derivation of effective transport coefficients of GDL, MPL and CCL
- **Methodology:** Multi-scale approach:
  1. MPL computation (FIB-SEM)
  2. GDL computation (X-ray Tom.)
  3. GDL/MPL assembly (X-ray Tom.)
  4. CCL computation (FIB-SEM)


**Inputs**
- MPL/GDL/Catalyst microstructure
- Material contact angles
- Catalyst and ionomer distribution
- Properties of the ionomer depending on the water content

→ DNS →

**Outputs**
- Volume averaged transport coefficients
- Effective contact angles

# Single layer scale

## 1. MPL computation (FIB-SEM)

- DNS using sequential approach
- Effective diffusion tensor has been computed
- $\frac{\partial c}{\partial t} = \nabla.(D(\boldsymbol{x})\nabla c)$ At pore scale
- $\frac{\partial C_{L_1}}{\partial t} = \nabla.(\epsilon(\boldsymbol{x})\boldsymbol{D_{L_1}}(\boldsymbol{x}).\nabla C_{L_1})$ At first Darcy-scale
- $\frac{\partial C_{L_2}}{\partial t} = \nabla.(\epsilon\, \boldsymbol{D_{eff}}.\nabla C_{L_2})$ At second Darcy-scale

- Same calculation method for thermal and electrical conductivity

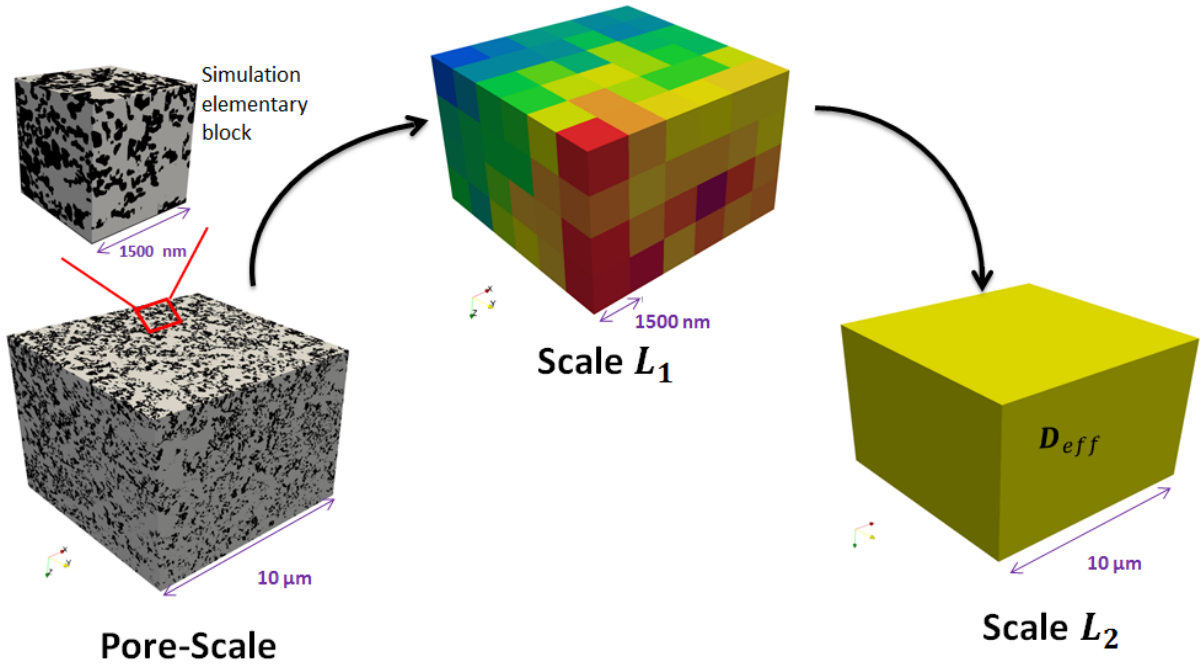

# Single layer scale

## 2. **GDL/MPL computation (X-ray Tomo.)**

- Cracked MPL reduces GDL diffusivity by 19% and uncracked MPL reduces GDL diffusivity by 25%

| | GDL without MPL | GDL with cracked MPL | GDL with uncracked MPL |
|---|---|---|---|
| Thinkness (µm) | 220 | 275 | 275 |
| Porosity | 0.88 | 0.81 | 0.80 |
| Through plane relative diffusivity ($1/\tau$) | 0.80 | 0.66 | 0.60 |
| $\frac{D_{eff}}{D_{bulk}}(=\frac{1}{\tau}) = (\frac{\epsilon-\epsilon_p}{1-\epsilon_p})^{\alpha}$ | 0.89 | - | - |
| $\frac{D_{eff}}{D_{bulk}}(=\frac{1}{\tau}) = \frac{1}{6}(\frac{4.7-1.7\epsilon}{2.7-1.7\epsilon} + \frac{9}{6.4-3.4\epsilon})$ | 0.88 | - | - |

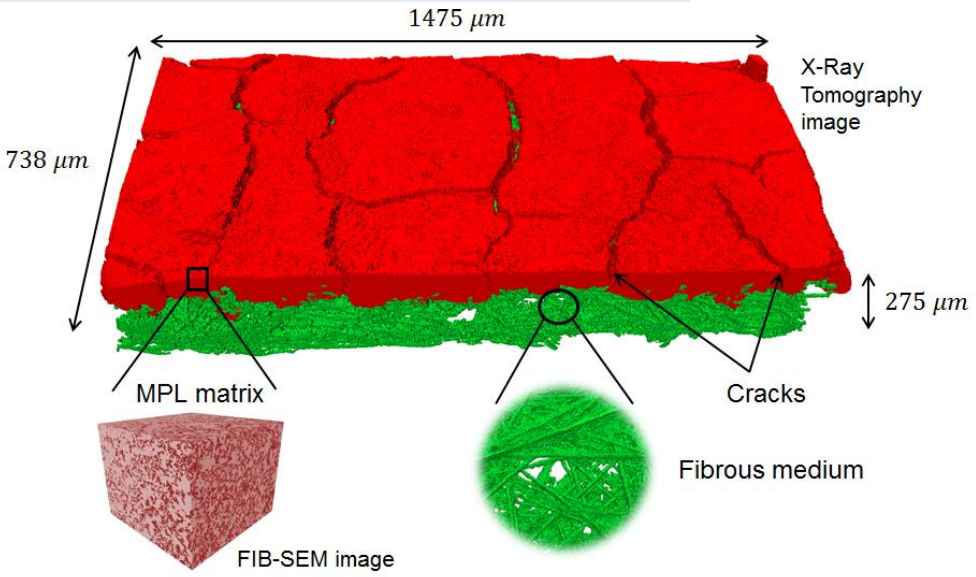


- GDL compression effect via resistance model

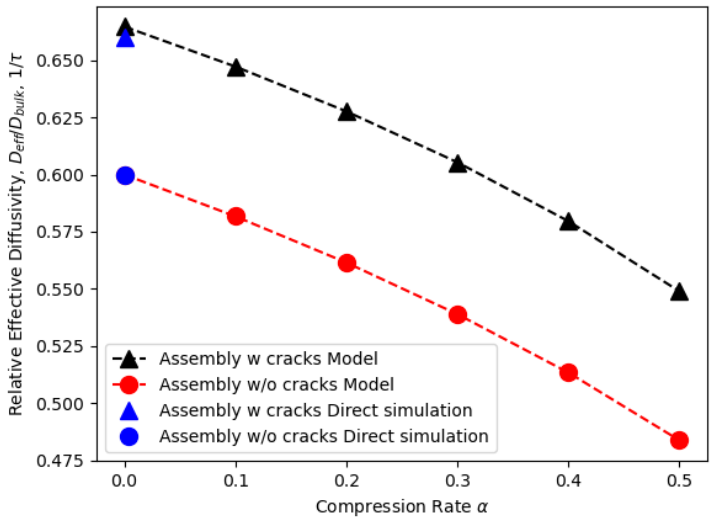

# Single layer scale

- **CCL computation:**
  - 3D reconstruction of CCL microstructure from FIB-SEM images
  - Ionomer reconstruction: ionomer partially occupying the pore space and ionomer thin films covering the carbon (in concave regions)
  - Computations of effective oxygen diffusion and effective proton conductivity tensors
    - Tensors are not isotropic
    - Knudsen diffusion has significant impact on oxygen diffusion
    - Liquid water in the primary pores found to have a significant impact

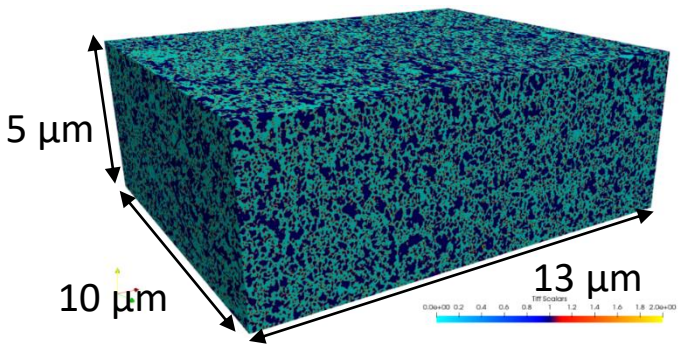


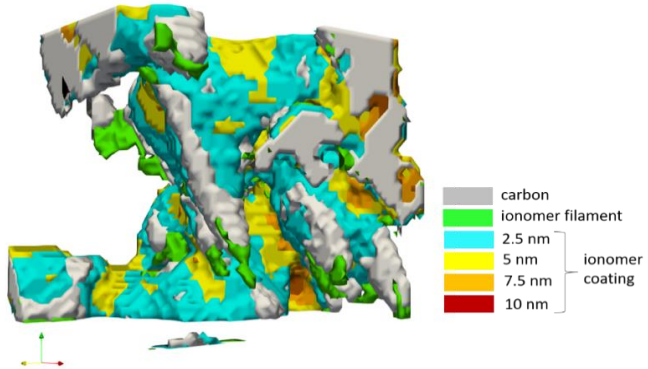


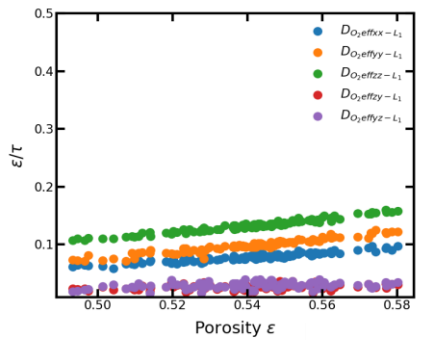


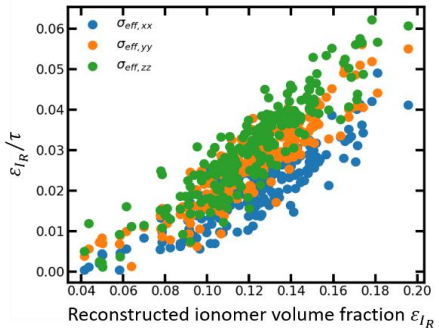


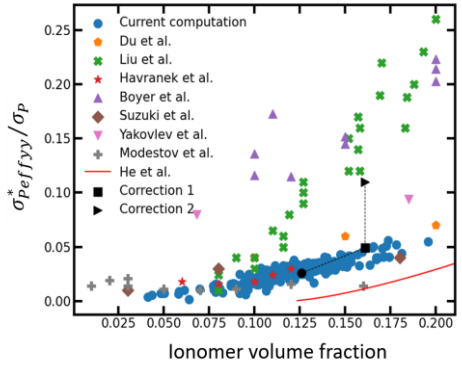

# Single layer scale

- **CCL computation:**
  - Pore size distributions calculated with Porespy[1]
  - Calculation of contact angle distribution: strongly dependent on ionomer distribution
  - Effective contact angles calculated at different scales suitable for two-phase flow DNS or PNM computations of important properties for macrohomogeneous models such as the water retention curve or the relative permeabilities
  - CCL water retention curve obtained

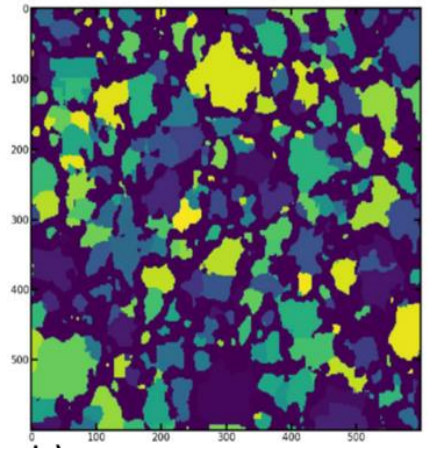

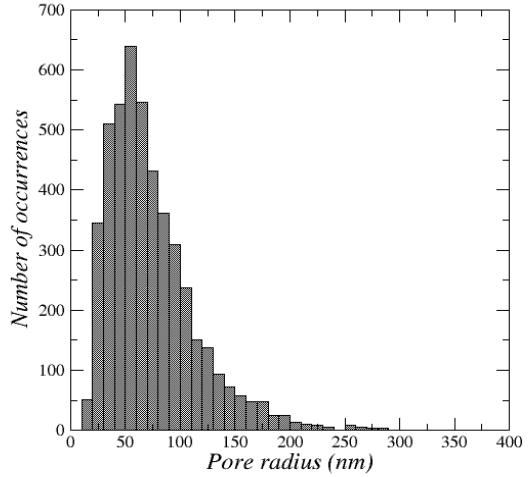


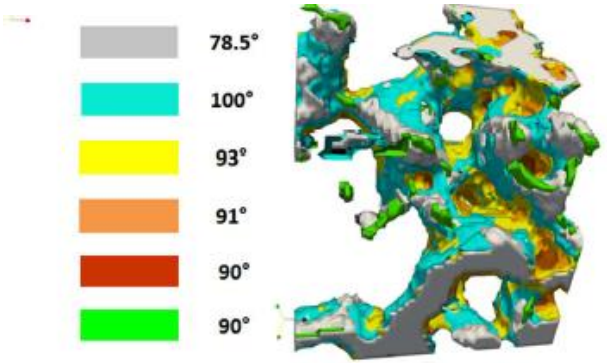


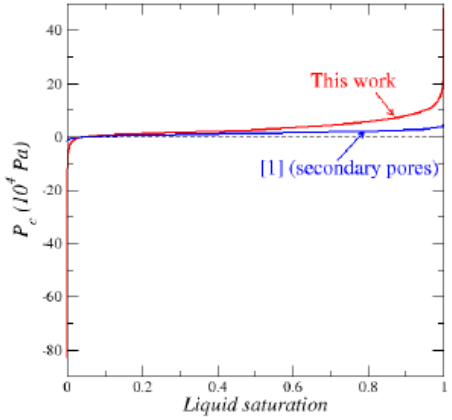


[1] J. Gostick et al. PoreSpy: A python toolkit for quantitative analysis of porous media images, Journal of Open Source Software, (2019).

# Cell scale

- **Objectives:**
  - Development and validation of single cell model including all relevant processes
  - Include improved sub-models and relations derived from lower scale models
  - Determination of the contributions of the different transport losses to the overall cell performance

**Inputs**
- Properties of cell components
- Local transport resistance distributions from LBM
- Effective Transport properties from single component scale
- Dedicated electrochemical measurements for model validation

→ Cell model →

**Output**
- Transient simulations of cell performance
- Identification of contributions to performance losses

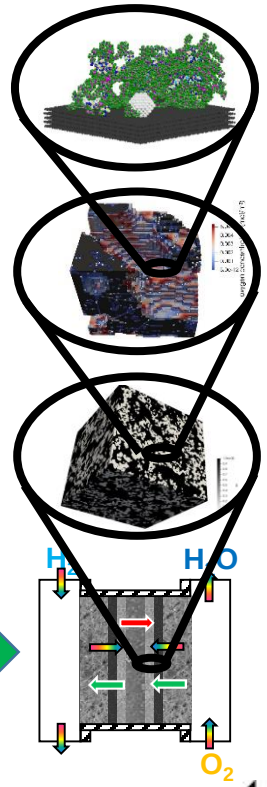

# Cell scale

- **Approach:**
  - Development of macro-homogeneous 2D multiscale cell model
    - Transient
    - 2D along-the-channel geometry
    - Mass, charge and energy transport
    - Novel ORR kinetics distinguishing between internal and external platinum and including surface coverage effects as well as local oxygen transport resistances
  - Implementation on DLR fuel cell modeling framework NEOPARD-X 2.0[1]
  - Use of effective transport properties derived from lower scale models
  - Parametrization and validation with dedicated ex-situ and in-situ experiments

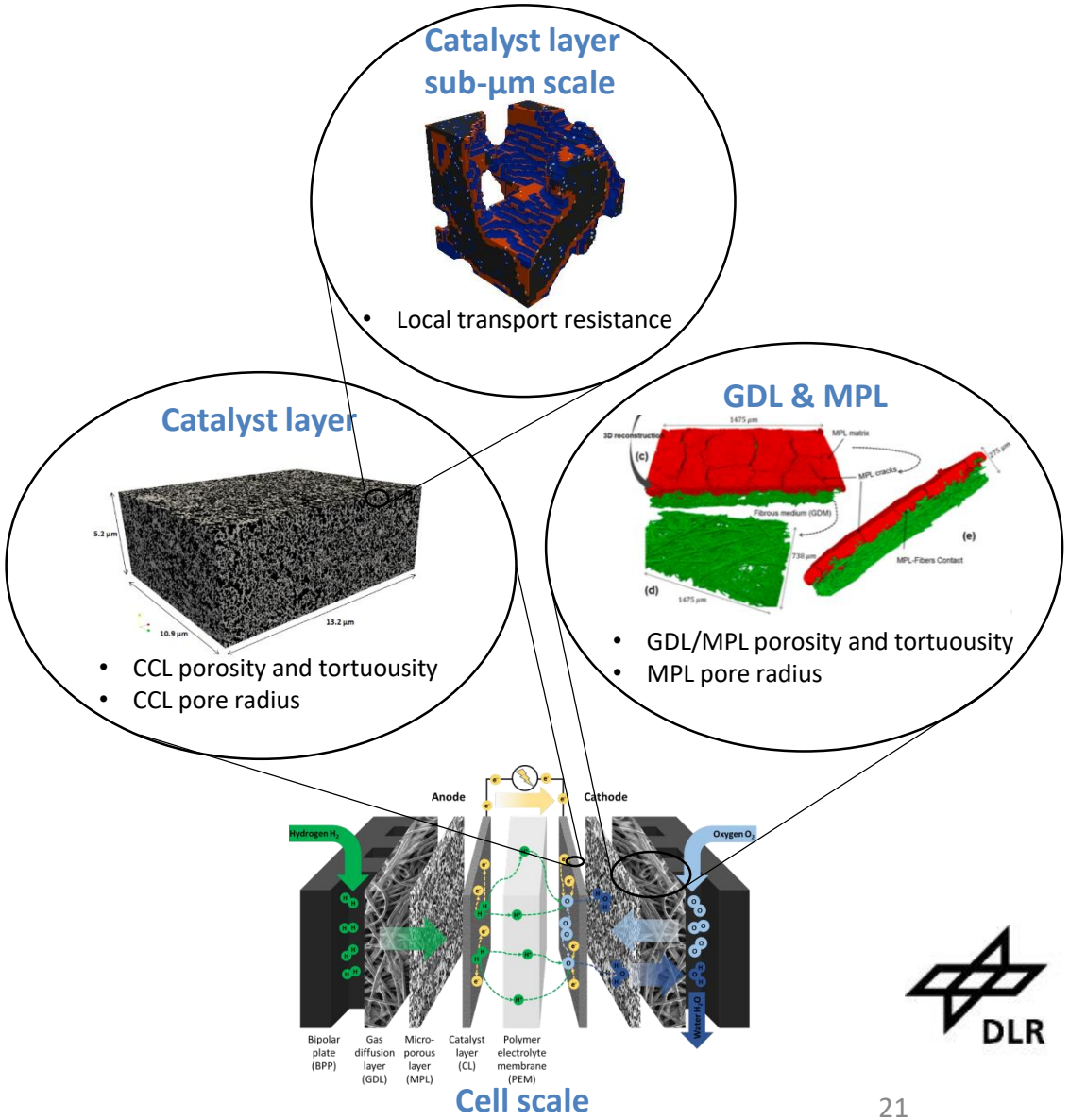


[1]: A. Koksharov, A. Latz, T. Jahnke, Electrochimica Acta 495 (2024) 144482

# Cell scale

**Transport models:**

- **Transport in channels:**
  - Free flow in channels described by Darcy-Brinkman
- **Transport in electrodes:**
  - Multicomponent mass transport in porous electrodes (diffusion + convection)
  - Charge transport (proton + electron) in electrodes
  - Energy transport: species enthalpy and heat conduction
  - Water sorption and transport in ionomer
- **Transport in PEM:**
  - Proton transport
  - Water diffusion and electroosmotic drag
  - Hydrogen crossover
- Effective diffusion coefficients obtained with lower scale DNS simulation

| | Model | Storage | Flux | Source | |
|---|---|---|---|---|---|
| Momentum | Darcy | $0$ | $0$ | $\mathbf{v} - (\nabla p - \rho \mathbf{g}) \frac{K}{\mu}$ | (17) |
| | Darcy-Brink. | $\varepsilon_g \rho \mathbf{v}$ | $\varepsilon_g (\rho \mathbf{v} \otimes \mathbf{v} + \mathbf{T} + \mathbf{S})$ | $\varepsilon_g \left(\rho \mathbf{g} - \nabla p - \mathbf{v} \frac{\mu}{K}\right)$ | (18) |
| Energy | | $\sum_{\alpha \in \Phi} \varepsilon_\alpha u^\alpha$ | $\varepsilon_g \left(\mathbf{v} \sum_{j \in g} c_j \bar{h}_j + \mathbf{T} \cdot \mathbf{v}\right) + \sum_{j \in S} \mathbf{j}_j \bar{h}_j - \kappa_{ef} \nabla T$ | $\mathbf{i}_{el} \cdot \nabla \varphi_{el} + \mathbf{i}_{ion} \cdot \nabla \varphi_{ion} - \bar{q}_{el} \mathcal{F} \Delta \varphi$ | (19) |
| Species $j$ | Gas phase g | $\varepsilon_g c_j$ | $\mathbf{v} \varepsilon_g c_j + \bar{\mathbf{j}}_j$ | $\bar{q}_j$ | (20) |
| | Other phase $\alpha$ | $\varepsilon_\alpha c_j$ | $\bar{\mathbf{j}}_j$ | $\bar{q}_j$ | (21) |
| Potential | Ionic | $-C_{dl} \Delta \varphi$ | $\mathbf{i}_{ion}$ | $-\mathcal{F} \bar{q}_{el}$ | (22) |
| | Electron | $C_{dl} \Delta \varphi$ | $\mathbf{i}_{el}$ | $\mathcal{F} \bar{q}_{el}$ | (23) |
| Ionomer water[1] | | $\varepsilon_\alpha \frac{\rho_{dry}}{EW} \frac{\partial \lambda}{\partial t}$ | $n_d \frac{\sigma}{F} \nabla \varphi_{ion} + \frac{\rho_{dry}}{EW} D_\lambda^{eff} \nabla \lambda$ | $q_\lambda$ | (24) |

Shear stress

$$\mathbf{T} = diag\left(\tfrac{2}{3}\mu \nabla \cdot \mathbf{v}\right) - \mu \left(\nabla \mathbf{v} + (\nabla \mathbf{v})^T\right) \quad (25)$$

Eddy viscosity

$$\mathbf{S} = -\rho \nu_{eddy} \left(\nabla \mathbf{v} + (\nabla \mathbf{v})^T\right) \quad (26)$$

Pressure

$$p = \mathcal{R}T \sum_{j \in g} c_j \quad (27)$$

Species flux

$$\bar{\mathbf{j}}_j = \sum_k D_{jk} \left(\nabla c_k + \frac{\mathcal{F}}{\mathcal{R}T} z_k c_k \nabla \varphi_{ion}\right) \quad (28)$$

Ionic current a)

$$\mathbf{i}_{ion} = \mathcal{F} \sum_j \bar{\mathbf{j}}_j z_j \quad (29)$$

Ionic current b)

$$\mathbf{i}_{ion} = -\sigma_{ion} \nabla \varphi_{ion} \quad (30)$$

Electonic current

$$\mathbf{i}_{el} = -\sigma_{el} \nabla \varphi_{el} \quad (31)$$

Potential step

$$\Delta \varphi = \varphi_{el} - \varphi_{ion} \quad (32)$$

| GDL/MPL properties (compressed)[1] | value |
|---|---|
| Thickness backing | 74 µm |
| Thickness MPL + overlap region | 76 µm |
| Porosity backing | 0.74 |
| Porosity MPL/overlap | 0.6072 |
| Tortuosity backing | 1.69 |
| Tortuosity MPL/overlap | 2.776 |
| Pore radius MPL | 150 nm |

| CCL properties | value |
|---|---|
| Thickness | 6 µm |
| Porosity[2] | 0.55 |
| Tortuosity[3] | 2.188 |
| Average pore radius[2] | 30 nm |
| Frac. of platinum in micropores | 70% |

# Cell scale

- **Novel approach for oxygen reduction reaction rate calculation:**
  - Distinguish between external platinum (covered by ionomer) and internal platinum (in micropores of the carbon)
    - $r_{\mathrm{ORR}} = r_{\mathrm{ORR}}^{\mathrm{int}} + r_{\mathrm{ORR}}^{\mathrm{ext}}$
  - Rate of ORR depends on local oxygen activity at platinum surface → determined by local transport losses
  - Integrate over contributions with distribution of local transport resistance $N(R_{\mathrm{Pt}})$

$$r_{\mathrm{ORR}}^{\mathrm{int/ext}} = \int_0^\infty N(R_{Pt}) r_{\mathrm{ORR}}^{int/ext}(R_{\mathrm{Pt}})\,\mathrm{d}R_{\mathrm{Pt}},$$

where $r(R_{Pt})$ is the solution of $r = k\left(a_{\mathrm{eq}} - r\frac{R_{Pt}}{C_{\mathrm{ref}}}\right)^{\gamma}$

    - Distribution $N(R_{\mathrm{Pt}})$ obtained from LBM on sub-µm scale
    - For each $R_{\mathrm{Pt}}$ reaction rate is calculated by analytical approximation[1]

$$\tilde{r}_{\mathrm{approx}} = k\frac{a_{\mathrm{eq}}^{\gamma}}{\left(1+\frac{a_{\mathrm{eq}}^{\gamma-1}}{A}\right)\left(1-4\Delta r_{\max}\frac{A_{\Delta r_{\max}}^{b}A^{b}}{\left(A_{\Delta r_{\max}}^{b}+A^{b}\right)^{2}}\right)}.$$

$$A := \frac{C_{\mathrm{ref}}}{k\,R_{\mathrm{local}}}$$

$$\Delta r_{max} = \frac{\gamma^{\frac{1}{\gamma-1}} - \gamma^{\frac{\gamma}{\gamma-1}}}{\left(\gamma^{\frac{1}{\gamma-1}}-1\right)\gamma^{\frac{\gamma}{\gamma-1}} + \gamma^{\frac{1}{\gamma-1}}}$$

$$A_{\Delta r_{\max}} = \frac{a_{\mathrm{eq}}^{\gamma-1}}{\gamma\left(\gamma^{\frac{1}{\gamma-1}}-1\right)}$$

$$b = \frac{\sqrt{2}\sqrt{-2\tilde{A} + 2\tilde{A}\Delta r_{\max} - \left(\tilde{A}+3\tilde{A}^2+3\tilde{A}^3+\tilde{A}^4\right)(\Delta r_{\max}-1)^2\beta}}{\sqrt{\Delta r_{\max}}\left(\tilde{A}+1\right)}$$

$$\beta = \frac{\gamma^{\frac{\gamma}{\gamma-1}}\left(\gamma-\gamma^2+2\gamma^{\gamma-1}(\gamma+2\gamma^2)-2\gamma^{\gamma-1}(\gamma-2\gamma^2)-\gamma^{\gamma-1}(\gamma+3\gamma^2-6\gamma^{\frac{2\gamma}{\gamma-1}}\right)}{\gamma^{\frac{3\gamma+2}{\gamma-1}}+3\gamma^{\frac{3}{\gamma-1}}(\gamma-2\gamma^2+\gamma^3)+\gamma^{\frac{2}{\gamma-1}}(1-3\gamma+3\gamma^2-\gamma^3)+3\gamma^{\frac{4}{\gamma-1}}(\gamma^2-\gamma^3)}$$

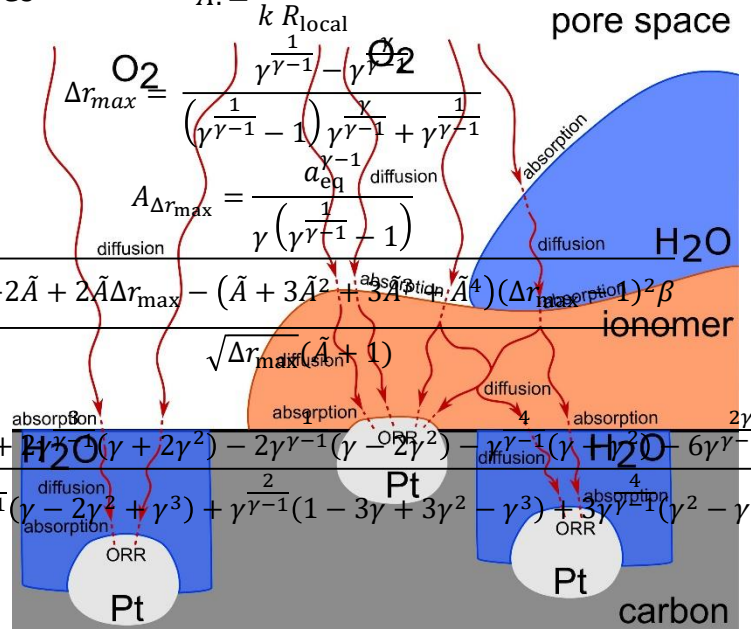


- **ORR kinetics** is described by modified Tafel kinetics with platinum oxide and ionomer coverage effect
  - Internal platinum:

$$k^{int} = i_0(1-\theta_{\mathrm{PtOx}})e^{-\frac{\omega\theta_{\mathrm{PtOx}}}{RT}}e^{-\frac{\alpha F}{RT}\eta}$$

  - External platinum:

$$k^{ext} = i_0(1-\theta_{\mathrm{PtOx}}-\theta_{\mathrm{ionomer}})e^{-\frac{\omega\theta_{\mathrm{PtOx}}}{RT}}e^{-\frac{\alpha F}{RT}\eta}$$

[1] Jahnke, T., Baricci, A. (2022), Journal of The Electrochemical Society, **169**, 094514

# Cell scale

- **Simulation of cell performance:**
  - **Hysteresis** observed potentiodynamic polarization curves can be accurately described by the model. Major contributions: Transient catalyst surface coverage with platinum oxides and ionomer
  - Same phenomena also responsible for **low frequency inductive features** in impedances → explain the discrepancy between Tafel slope and experimentally observed low frequency resistance
  - **Local transport resistance distribution** leads to transport related performance losses already at low current densities!

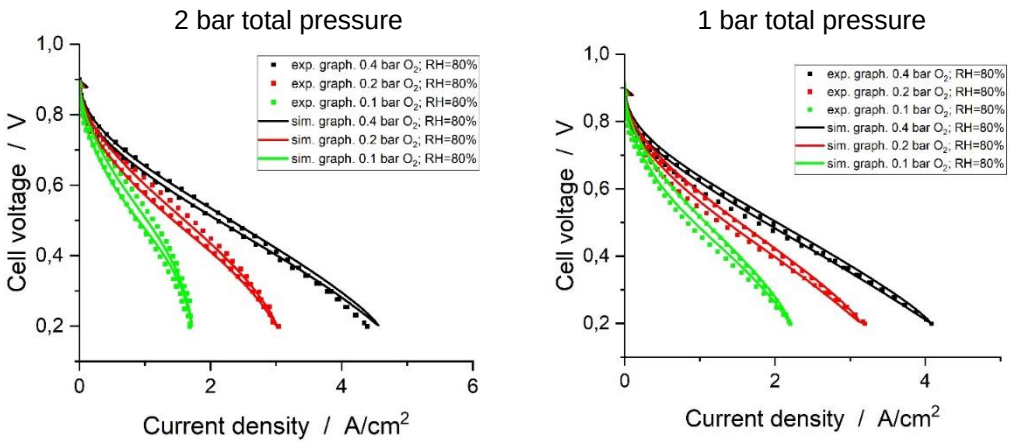


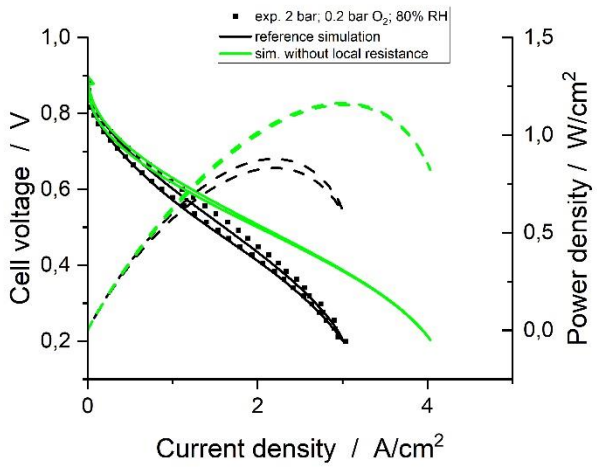


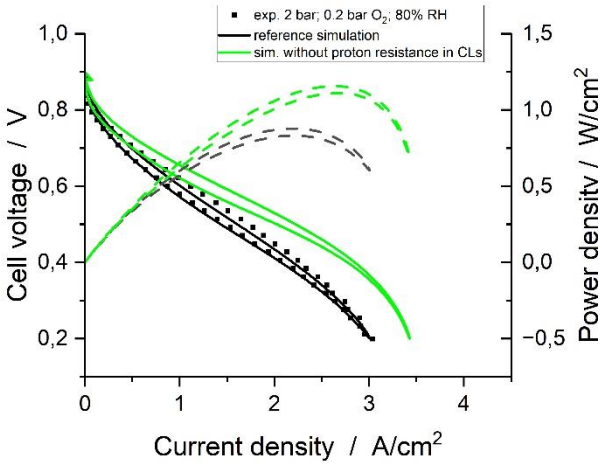


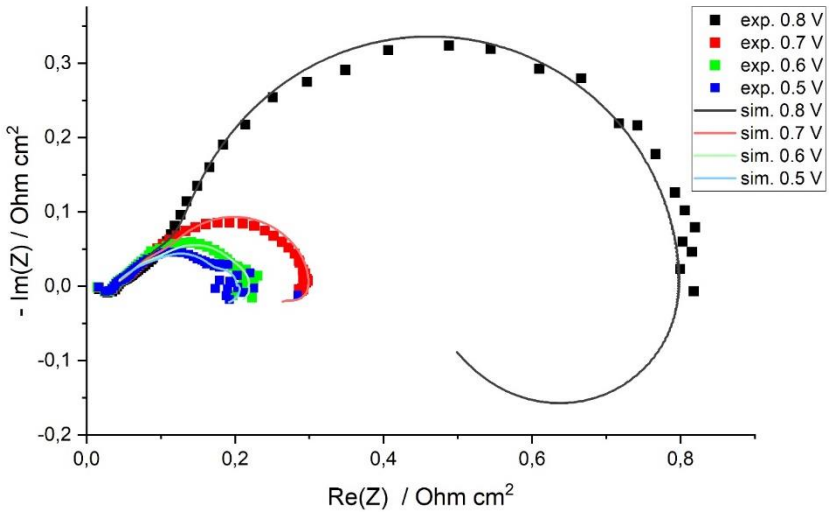

# Cell scale

- **Break down of transport resistance contributions at limiting current:**
  - Determine local oxygen concentrations at layer interfaces
  - Calculate local $R_{\mathrm{O2,local}}$ for each layer $l$

$$R_{\mathrm{O2,local}} = \frac{4F\Delta c_l}{i_{local}}$$

  - Channel contribution important even at high flow rate (6 Nl/min ≙ λ=10 @3A/cm$^2$ in air) due to parabolic velocity profile
  - CCL contribution strongly dependent on RH
  - CCL contribution decreases from inlet to outlet (better humidification)

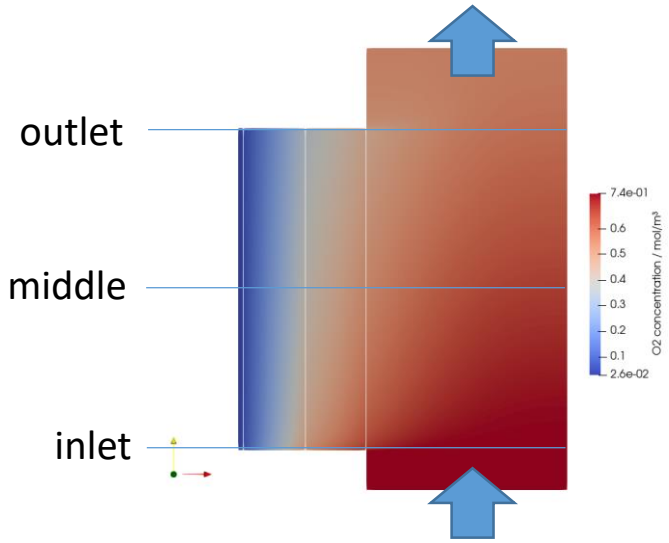


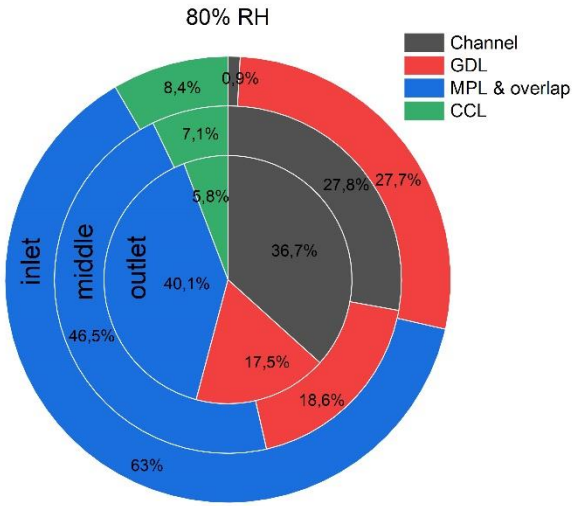


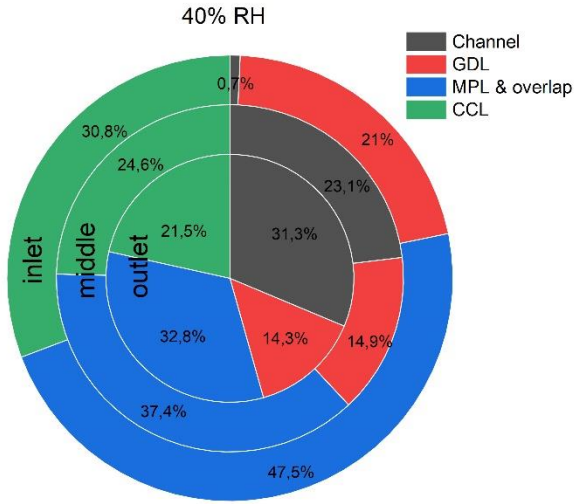

# Cell scale

- Simulation of **polarization curves under LCA conditions** (2% oxygen; 80% RH; 80°C)
- “Knee” in polarization curve caused by transport limitations for internal platinum
- Very sensitive to distribution of interfacial resistance between ionomer|gas and ionomer|platinum interfaces
- Good agreement with LCA can be achieved with main contribution at ionomer|gas interface
- EIS simulation confirms accurate representation of processes

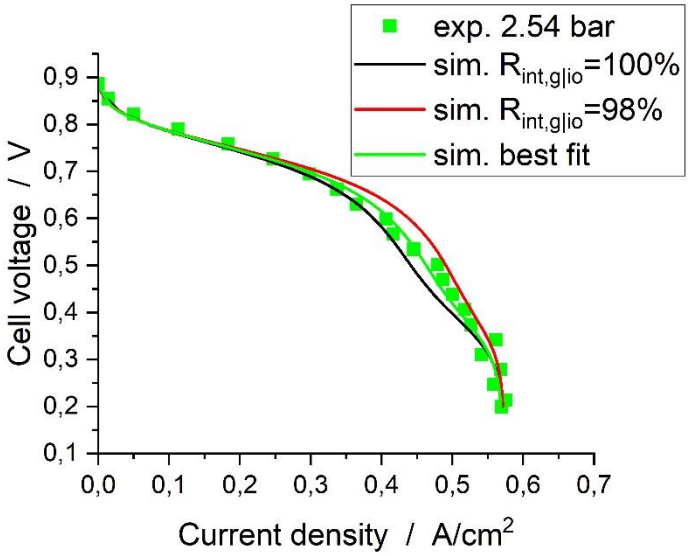


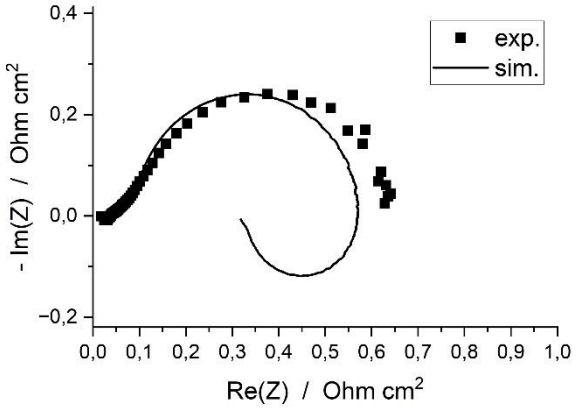


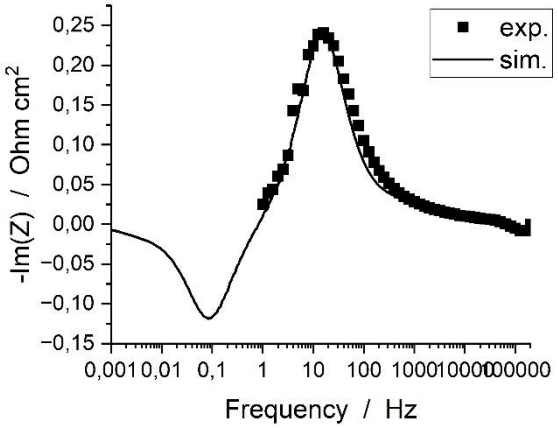


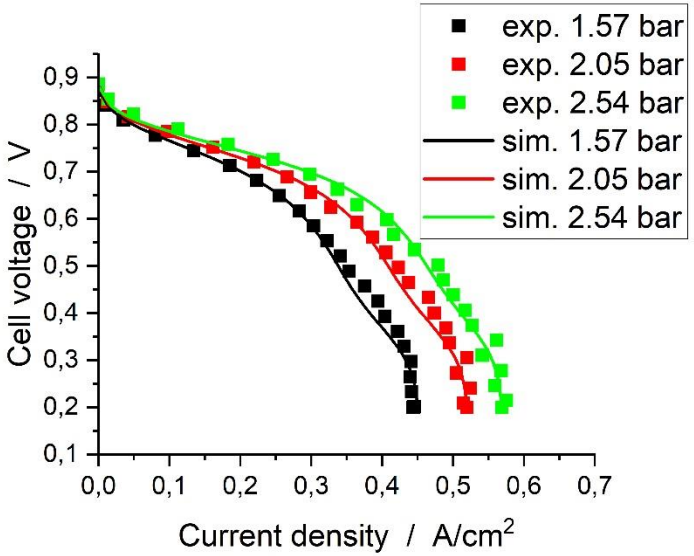


Impedance at 2 bar; 0.1 bar $O_2$; 80% RH; 0.8V

# Cell scale

**Comparison graph. carbon vs. HSAC:**

- Significantly lower voltage at low currents but higher limiting current
- LCA: significantly lower pressure dependent part probably due to inhomogeneity in GDL properties

**Major differences in model parameters:**

- No platinum in micropores; lower ECSA; ORR kinetics; GDL/MPL tortuosities
- Approx. 36% higher transport resistance for external Pt
- Hypothesis: higher platinum content at carbon surface as well as different carbon surface properties lead to different ionomer orientation → $SO_3$ groups towards platinum surface

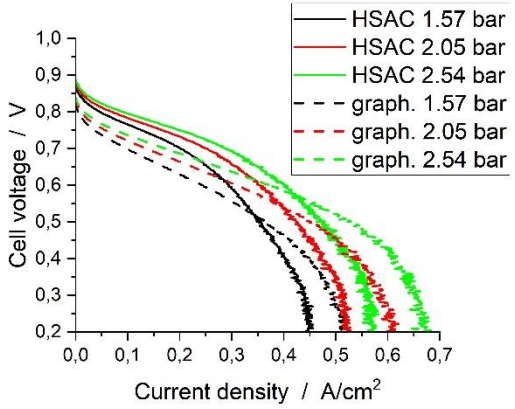


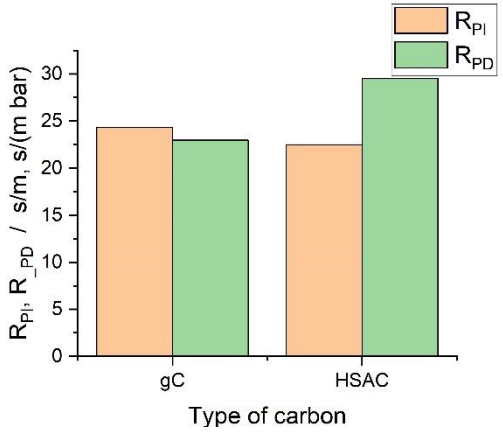


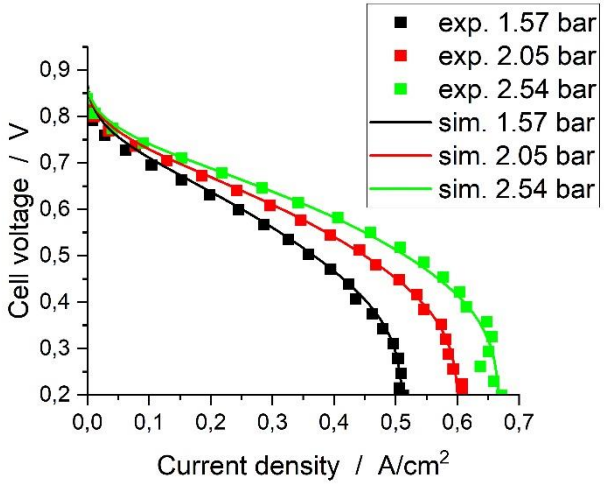


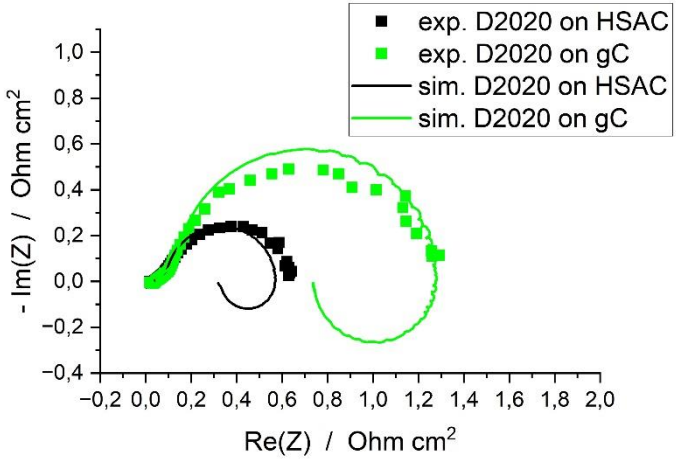


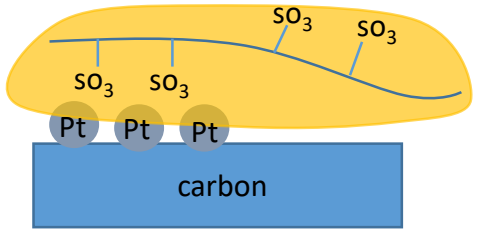

# Cell scale

**Comparison HOPI vs. D2020:**

- Higher catalyst activity
- More sudden transport limitation at higher currents

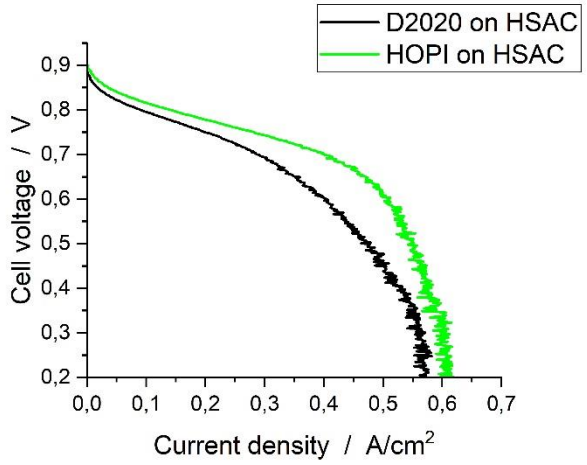


**Major differences in model parameters:**

- Lower Henry constant ($c_{eq} = c_g/H$) for HOPI → higher $O_2$ conc. at catalyst
- Higher activity of external platinum
- Higher transport resistance for external platinum
- Significantly lower transport resistance for internal platinum
- Hypothesis: shift of interfacial resistance towards platinum interface

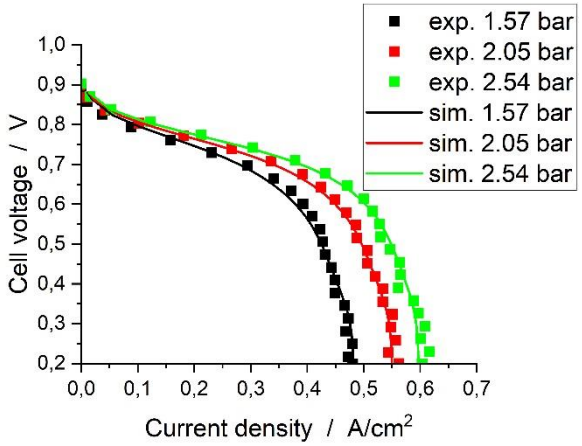


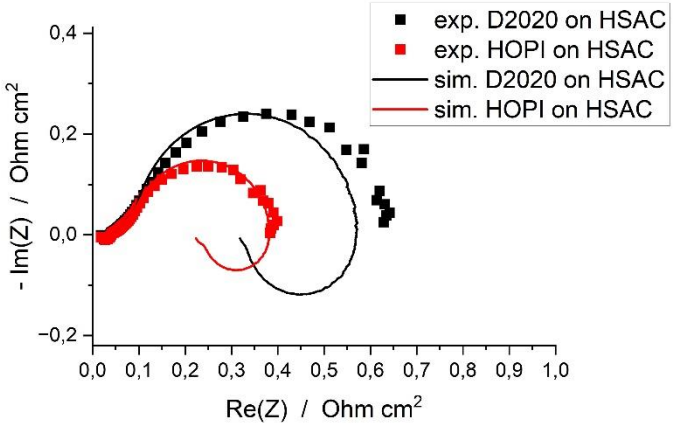


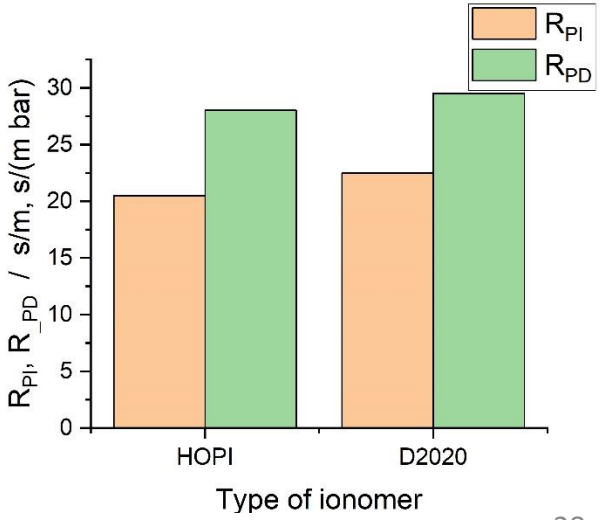

# Multiscale-modeling: conclusions

**Development of multiscale modeling methodology to link material properties with cell performance**

- **Molecular Dynamics simulation of ionomer film:**
  - Simulation of ionomer self-assembly, solvent effects and solvent evaporation
  - Preliminary results on oxygen and water distributions in ionomer film
- **Lattice Boltzmann modeling of the CCL on sub-µm scale:**
  - Reconstruction of realistic CCL structures
  - Simulation of oxygen transport and derivation of local transport resistance distribution
- **DNS on GDL, MPL and CCL microstructures:**
  - 3D reconstructions of GDL, MPL and CCL
  - Derivation of effective transport properties for oxygen, water and protons
- **Volume averaged cell model**
  - Coupling of transport processes in all layers and electrochemistry in a 2D cell model
  - Use of effective transport properties of lower scale models and novel formulation of ORR kinetic
  - Enables description of transient behavior such as hysteresis and EIS
  - Was used for breakdown of transport losses and to compare different CCL materials

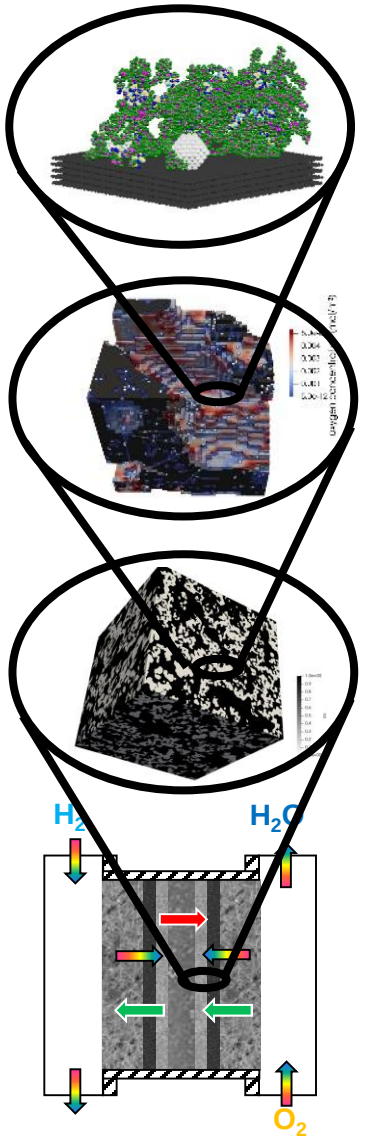


UNIVERSITY OF CALGARY

DLR

INP TOULOUSE

DLR

# The TEAM

Dr. Laure Guetaz

Dr. Pascal Schott

PhD Konrad Guelicher

Dr. Isotta Cerri

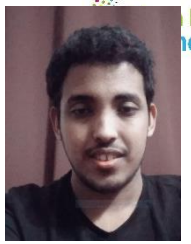

PhD Ahmed Maloum

Dr. T. B. Hue Tran

Dr. Arnaud Morin

Dr. Joël Pauchet

Dr. Jens Mitzel

Dr. Thomas Jahnke

Pr. Anthony Kucernak

Dr. Colleen Jackson

Dr. Stéphane Cotte

Dr. Aurélie Gueguen

Dr. Michel Quintard

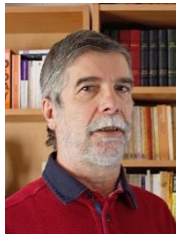

Dr. Marc Prat

PhD Florian Chabot

| | | | | |
|---|---|---|---|---|
| liten ceatech | Deutsches Zentrum für Luft- und Raumfahrt German Aerospace Center | Imperial College London | TOYOTA | INP TOULOUSE |
| Université Montpellier / iem | PAUL SCHERRER INSTITUT PSI | ESSLINGEN UNIVERSITY | Chemours | UNIVERSITY OF CALGARY |

Dr. Jason Richard

Dr. Stefano Deabate

Pr. Patrice Huguet

Dr. Pierre Boillat

Dr. Jong Min Lee

Pr. Hanno Kaess

Dr. Tobias Morawietz

Patrick Redon

Pr. Kunal Karan

PhD Afeteh Tarokh

Dr. Dirk Scheuble

This project has received funding from the Fuel Cells and Hydrogen 2 Joint Undertaking (now Clean Hydrogen Partnership) under Grant Agreement No **875025**. This Joint Undertaking receives support from the European Union's Horizon 2020 Research and Innovation program, Hydrogen Europe and Hydrogen Europe Research.